RSC Advances

PAPER

View Article Online
View Journal | View Issue

Cite this: *RSC Adv.*, 2022, **12**, 17817

Enhanced healing process of tooth sockets using strontium-doped TiO_2†

Jialing Li,[ab] Zilu Fan,[b] Min Huang,[b] Yonglin Xie,[b] Zhenju Guan[b] and Jianping Ruan *[a]

Received 18th January 2022
Accepted 20th May 2022

DOI: 10.1039/d2ra00341d

rsc.li/rsc-advances

Prevention of residual ridge resorption is important for tooth socket healing in clinical treatment. As a well known biomaterial, titanium dioxide (TiO_2) has been reported to show desirable bone regeneration capability. On the other hand, strontium plays a role in maintaining normal function in organisms and balancing bone remodeling. Hence, we synthesized strontium-doped titanium dioxide mesoporous nanospheres functionalized with amino-group using diphenyl diisocyanate. After incorporation with segmented polyurethane, the obtained injectable SPU/Sr-TiO_2/MDI nanocomposite adhesive showed satisfactory antibacterial activity and cell nontoxicity. This nanocomposite was used for tooth socket healing, and greatly promoted the formation of new bone tissue in the tooth extraction socket.

Residual ridge resorption (RRR), which is the resorption of alveolar bone after tooth extraction, is an irreversible, progressive, chronic, and cumulative process.[1,2] RRR always contributes to various aesthetic issues in edentulous patients, thus the prevention or reduction of the RRR process after tooth extraction is of great significance in clinical treatment.[3,4] In theory, one possible strategy is the implantation of autologous bone organization into the extracted tooth socket. Nevertheless, it is challenging for this treatment to fit the irregular shape of an extracted socket, which can further bring a secondary injury.[5,6] Recently, several synthetic biomaterials (*e.g.* tricalcium phosphate and hydroxyapatite) have been transplanted into extraction sockets to enhance bone formation.[7–10] These materials preliminarily display satisfactory biocompatibility, osteoinductivity, and bioactivity. However, their degradation rate can't perfectly meet the demand of the regeneration rate of new bone. In this regard, it is necessary to present a deeper understanding and design of an effective biomaterial system for facilitating socket healing and reducing RRR.

As a widely investigated biomaterial, nanoscale titanium dioxide (TiO_2) with unique physical and chemical properties has been used for diverse fields such as photocatalysis, energy storage and conversion, wound healing, and bone generation.[11–15] Recent research by Lin *et al.* verified that the TiO_2 based material on magnesium implants is able to greatly suppress bacterial infection and promote new bone formation.[16] Some other studies have demonstrated that the combination of nano TiO_2 into polymer scaffolds can achieve high mechanical property and desirable bioactivity.[17–21] Recently, Ikono *et al.* fabricated hybridized chitosan sponges incorporated with anatase-type TiO_2 nanoparticles for bone tissue engineering.[22] Cytotoxicity analysis confirmed the biocompatibility of chitosan/TiO_2 sponges, and qPCR analysis revealed their bone regeneration capability. The group of Mohd reported the preparation of TiO_2/gellan gum composite biofilm with excellent cell viability, antibacterial property, and cell proliferation as wound dressing material.[23] Despite extensive studies of nanoscale TiO_2 have been reported, its discussion and application in tooth socket repair are still limited.

In recent years, much attention are focused on applying trace elements into implants in order to modify in osteogenesis and improve bone bonding, and most of them have achieved impressive results. Strontium is one of the essential trace elements in the bone and plays an important role in maintaining the balance of bone function. Many studies have proved that strontium can induce bone marrow mesenchymal stem cells to differentiate into osteoblast, promote the proliferation of osteoblasts as well as secrete osteoblast matrix, and inhibit the proliferation of osteoclasts and bone resorption.[24–26] Therefore, strontium deserves to be intensively studied in the process of bone mineralization.

In this study, Sr-doped TiO_2 mesoporous nanospheres were fabricated using a facile hydrothermal process, which were then functionalized with amino-group and displayed improved antibacterial activity. Subsequently, we incorporated the NH_2-functionalized Sr/TiO_2 (Sr-TiO_2/MDI) nanospheres into the segmented polyurethane (SPU) scaffold. The obtained injectable SPU/Sr-TiO_2/MDI nanocomposite shown desirable cell nontoxicity and biocompatibility. Significantly, the SPU/Sr-TiO_2/MDI adhesives presented higher repair effect for tooth socket compared to the controlled SPU group. It greatly

[a]*College of Stomatology, Department of Preventive Dentistry, Xi'an Jiao Tong University, Xi'an, Shaanxi, People's Republic of China. E-mail: jianpingruan@126.com*
[b]*Nanchong Central Hospital, The Second Clinical College of North Sichuan Medical College, Nanchong, Sichuan, People's Republic of China*

† Electronic supplementary information (ESI) available. See https://doi.org/10.1039/d2ra00341d

promoted the formation of new bone tissue in tooth extraction socket after 4 weeks of treatment. This study suggests that the SPU/Sr-TiO_2/MDI nanocomposite is a promising candidate for bone repair and formation in tooth socket treatment.

The microscopic morphology of the as-synthesized Sr-doped mesoporous TiO_2 products were characterized by SEM technique. As shown in Fig. 1(a and b), the Sr-TiO_2 presents a uniform sphere-like nanostructure with the diameter of 200–300 nm (Fig. 1(c)). The TEM images in Fig. 1(d) reveal the Sr-TiO_2 nanospheres are composed of a large number of nanoparticle with the size of around 20–30 nm, forming massive mesopores for Sr-TiO_2 nanospheres, as marked using red circle in Fig. 1(e). As provided in Fig. 1(f), the BET surface area was measured as 118.4 $m^2\ g^{-1}$, and the diameter of the mesopores were centered at 3–8 nm, which is consistent with the TEM result. The Sr-TiO_2 nanospheres with interconnected mesoporous structure and high surface area are of great importance for improving their bioactivity in the following study. It is observed distinctive lattice fringes from the HRTEM image in Fig. 1(g), suggesting the prepared Sr-TiO_2 nanospheres are crystalline. The interplanar spacing of 0.351 nm is assigned to (101) plane of anatase phase TiO_2.[27] Fig. 1(h–j) provide the energy dispersive X-ray spectroscopic (EDS) mapping images of Sr-TiO_2 mesoporous nanospheres. The element of Ti, O, and Sr are homogeneously distributed within the sample, indicating the successful doping of Sr in the TiO_2 structure.[27,28]

We prepared various Sr-doped TiO_2 products by varying the amount of $Sr(NO_3)_2$. The Sr doping content was determined by the inductively coupled plasma atomic emission spectrometry (ICP-AES) method. Fig. S1(a)† shows the XRD profiles of TiO_2, 0.1 Sr-TiO_2, 0.2 Sr-TiO_2, and 0.3 Sr-TiO_2 products. All samples present similar characteristic peaks located at $2\theta = 26°, 37°, 47°, 54°, 55°, 63°, 70°, 72°$, and $75°$, they are indexed to the (101), (004), (200), (105), (211), (204), (116), (220), and (215) planes of the anatase phase TiO_2 (JCPDS card no: 21-1272).[22,29] The TiO_2 crystal structure is not obviously changed after doping with Sr. The Raman spectra of various products are given in Fig. S1(b).† It is observed the main distinct band centered at 143 cm^{-1} accompanied with several low bands at 202 cm^{-1}, 394 cm^{-1}, 517 cm^{-1}, and 638 cm^{-1}. The characteristic band of 143 cm^{-1} is attributed to the E_{g1} phonon mode of the anatase TiO_2.[30] We can find the slightly broadening and blue shift of E_{g1} band for Sr doped samples compared to the undoped TiO_2. The possible reason is the Sr-doping can increase the non-stoichiometry and phonon confinement of the mesoporous TiO_2 induced by strain and defects.[31]

To present a better understanding of the Sr doped TiO_2 sample, XPS technique was performed to obtain the chemical states of different elements. The XPS survey spectrum in Fig. S2(a)† reveals the presence of O, Ti, and Sr in Sr doped TiO_2 mesoporous nanospheres. Fig. S2(b)† shows the high-resolution XPS pattern of the Ti 2p, the two characteristic bands at 464.5 eV and 458.8 eV stand for Ti $2p_{1/2}$ and $2p_{3/2}$ of Ti(IV) in TiO_2, respectively. For Sr-doped TiO_2 samples, we can observe a shift of around 0.4 eV for Ti $2p_{3/2}$ band.[32] As shown in Fig. S2(c),† the high-resolution spectrum of the O 1s for Sr-doped TiO_2 sample was deconvoluted into two bands of 530.5 eV and 530.5 eV that presented the lattice oxygen and oxygen vacancy, respectively. Further more, the Sr 3d spectrum (Fig. S2(d)†) contains two bands of 135.2 eV and 133.6 eV, which correspond to the Sr $3d_{5/2}$ and Sr $3d_{3/2}$, respectively, confirming that the Sr has been successfully presented as dopants in the mesoporous TiO_2 nanospheres.[33]

The as-characterized 0.2 Sr-TiO_2 sample was used for following study. The synthetic process of the NH_2-functionalized Sr-TiO_2 mesoporous nanospheres were illustrated in Fig. 2(a). Firstly, the –NCO group of MDI can react with –OH on the surface of Sr-TiO_2 nanospheres. Next, the unreacted –NCO was hydrolyzed to form the NH_2-functionalized products. In this research, MDI functions as not only the surface modifier, but also the starting monomer for SPU polymer. As can be seen in

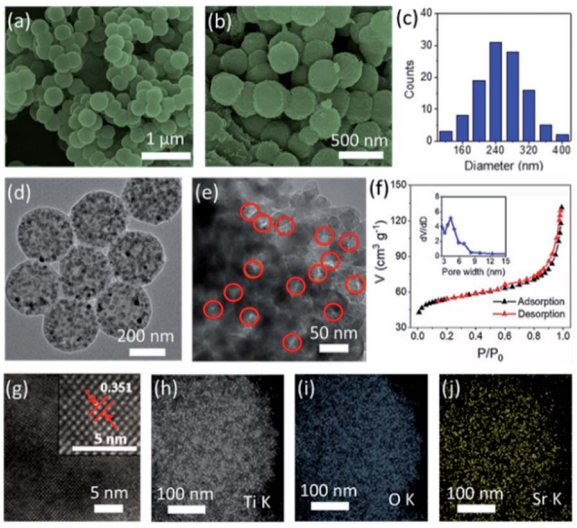

Fig. 1 (a and b) SEM images of Sr-doped mesoporous TiO_2 nanospheres. (c) Diameter distribution of Sr-doped mesoporous TiO_2 nanospheres. TEM (d and e), BET profile (f), and HRTEM (g) images of Sr-doped mesoporous TiO_2 nanospheres. (h–j) Elemental mapping images of Ti, O, and Sr K.

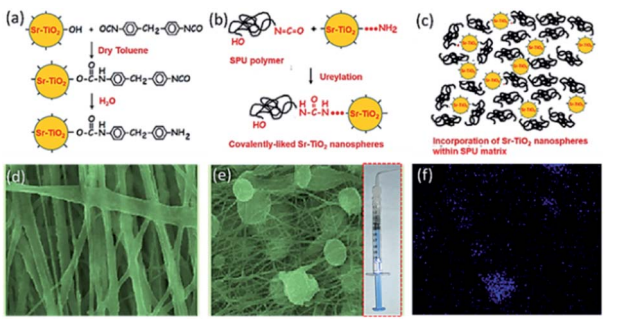

Fig. 2 (a) Synthetic process of the NH_2-functionalized Sr-TiO_2-mesoporous nanospheres. (b) Reaction between SPU macromolecules and NH_2-functionalized Sr-TiO_2 nanospheres. (c) Illustration of the injectable polymeric SPU matrix incorporated with NH_2-functionalized TiO_2 nanoparticles Sr-TiO_2 nanospheres. SEM images of SPU matrix (d) and (e) SPU/Sr-TiO_2/MDI composite. (f) Elemental mapping of Ti.

Fig. 2(b), SPU macromolecules can be connected to the NH_2-functionalized Sr-TiO_2 mesoporous nanospheres through the generation of urea linkages. Additionally, the NH_2-functionalized Sr-TiO_2 nanospheres are able to act as more chain extenders for SPU macromolecules because they have a large number of amine terminal groups (Fig. 2(c)), leading to the homogenous distribution of Sr-TiO_2 nanospheres within the injectable polymeric SPU matrix. The as-prepared injectable SPU/Sr-TiO_2 composite were investigated by the SEM technique. Compared to the SPU polymer matrix (Fig. 2(d)), we can observe uniform dispersion of Sr-TiO_2 mesoporous nanospheres inside the SPU scaffold (Fig. 2(e)), which was also confirmed by the EDS mapping image of Ti element in Fig. 2(f).

Fig. S3(a)† depicts the XRD profiles of TiO_2, Sr-TiO_2, SPU/Sr-TiO_2/MDI, SPU/Sr-TiO_2, and SPU samples. As a polymeric material, the pure SPU sample displays a broad peak at around 21°, indicative of its amorphous nature.[34] The characteristic peaks of Sr-TiO_2 nanospheres can be observed in the composites of SPU/Sr-TiO_2/MDI and SPU/Sr-TiO_2, suggesting the presence of Sr-TiO_2 in the polymeric SPU scaffold. The SPU/Sr-TiO_2/MDI nanocomposite was further studied by recording its UV-vis DR spectrum with the wavelengths ranging from 300 to 800 nm. As depicted in Fig. S3(b),† Sr-TiO_2 presents a wider optical absorption above 400 nm compared to undoped TiO_2. As expected, the incorporation of Sr-TiO_2 mesoporous nanospheres into the polymeric SPU can greatly improve the light absorption in the UV range of 300–400 nm.

The growth activity of cells on the surface of each material was detected by living/dead cell staining 72 h after inoculation, cells on the surface of material were stained with Calcein-AM and PI. The staining images as well as quantitative analysis are shown in Fig. S4 and S5,† respectively. A large number of Calcein-AM green stained living cells were seen on the surface of both materials, while only sporadic red stained dead cells were seen. It shows that both materials have fine biocompatibility, and the number of cells in SPU/Sr-TiO_2/MDI group is higher than that in SPU group.

Because of the improved antibacterial activity and cell viability of SPU/Sr-TiO_2/MDI nanocomposite adhesive, its socket repair effect has been studied and compared with the controlled SPU group. Fig. 3 shows histological images of rat extraction socket from 1 week to 7 weeks after treatment. In the SPU/Sr-TiO_2/MDI group, the histological result demonstrates that width of newly formed bone tissue gradually increase with time in the extraction socket. A large number of spindle stromal cells together with few inflammatory cells were found infiltrated in extraction socket after 1 week. Additionally, there are sparse woven bones and a small amount of osteoblasts infiltrated in the extraction socket at 2 weeks. At week 4, it is observed denser newly formed alveolar bone surrounded by inflammatory cells, while only little new formed bone tissue was detected for SPU group. After 7 weeks of treatment, we can observe significant bone formation in SPU/Sr-TiO_2/MDI group, most of extraction sockets are occupied by the newly formed bone tissue. However, little bone formation is observed in the extraction socket treated with controlled SPU group, and there are apparent gaps exist among the newly formed bone tissues. It is worth noting that the injectable SPU/Sr-TiO_2/MDI adhesive presents a fast degradation rate in the extraction socket, enabling the promoted process of bone tissue formation.[35]

To provide a further understanding of socket repair effect of SPU/Sr-TiO_2/MDI adhesive, the bone density of all mandible samples was determined and analyzed. The soft X-ray photographs of tooth socket treated with control SPU and SPU/Sr-TiO_2/MDI adhesive are shown in insets of Fig. 3. The newly formed trabecular bone for SPU/Sr-TiO_2/MDI group is wider than controlled SPU group after 7 weeks of operation. Fig. 4 provides optical density of newly formed bone tissue in the tooth socket. It is found that bone mineral density of the extraction socket treated with SPU/Sr-TiO_2/MDI is higher than that of the controlled SPU group after a week. Significantly, the bone density bas been greatly increased until 7 weeks for SPU/Sr-TiO_2/MDI, while the bone density is quite stable for SPU group and only a slight increase is observed from 4 weeks to 7 weeks. The above findings and analyses reveal the existence of both bone formation and resorption in the process of tooth socket repair, indicating the satisfactory repair effect of the prepared SPU/Sr-TiO_2/MDI nanocomposite adhesive. Furthermore, we have compared SPU/Sr-TiO_2/MDI with some mainstream materials in this field, summarized in Table S1.† Despite the long-term durability requires to be observed, SPU/Sr-TiO_2/MDI have many merits like anti-infection, suitable for periodontitis extraction of affected teeth, injectability, strong

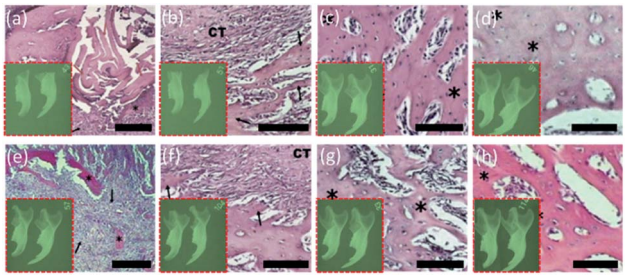

Fig. 3 Histological images and soft X-ray photographs (insets) of tooth socket treated with control SPU after 1 week (a), 2 weeks (b), 4 weeks (c), and 7 weeks (d). Histological images and soft X-ray photographs (insets) of tooth socket treated with SPU/Sr-TiO_2/MDI adhesive after 1 week (e), 2 weeks (f), 4 weeks (g), and 7 weeks (h). Scale bar: 100 μm.

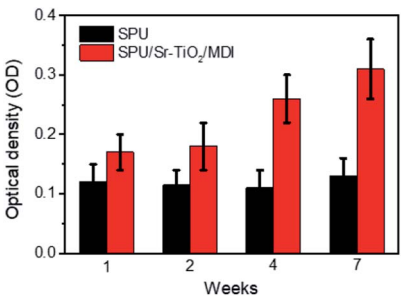

Fig. 4 Quantitative analysis of newly formed bone tissue in the socket treated with control SPU and SPU/Sr-TiO_2/MDI adhesive.

plasticity, and convenient operation. It is very suitable for post extraction site preservation of irregular extraction socket and hard to cause secondary injury of bone repair site.

Conclusions

In summary, Sr-doped TiO_2 mesoporous nanospheres with uniform size were fabricated using a facile hydrothermal process, which were functionalized with amino-group and incorporated into SPU matrix through the urea linkages to obtain injectable SPU/Sr-TiO_2/MDI adhesive. The resulted nanocomposite shown desirable antibacterial activity and cell nontoxicity. As the repair adhesive for tooth socket, the SPU/Sr-TiO_2/MDI is able to greatly promote the formation of new bone tissue in tooth extraction socket after 4 weeks of treatment. By contrast, little bone generation was observed in the extraction socket treated with controlled SPU group. Therefore, the as-studied SPU/Sr-TiO_2/MDI nanocomposite is a promising candidate for bone repair and formation in tooth socket treatment.

Conflicts of interest

There are no conflicts to declare.

Acknowledgements

This study was supported by the National Natural Science Foundation of China (81670985), City-School Strategic Cooperation Science Foundation of China Nanchong (18SXHZ0476), and Science Foundation of North Sichuan Medical College (CBY18-A-YB33).

References

1 S. Gupta, S. V. Singh and D. Arya, *Polymorphism*, 2019, **2**, 107–113.
2 O. P. Singh, R. Kaur, S. M. Nanda and E. Sethi, *Indian Journal of Oral Sciences*, 2016, **7**, 3.
3 Y. Maruo, G. Nishigawa, M. Irie, M. Oka, T. Hara, K. Suzuki and S. Minagi, *Arch. Oral Biol.*, 2010, **55**, 873–878.
4 N. Tymstra, G. M. Raghoebar, A. Vissink and H. J. A. Meijer, *J. Oral Rehabil.*, 2011, **38**, 509–516.
5 M. Paolantonio, M. Dolci, A. Scarano, D. d'Archivio, G. Di Placido, V. Tumini and A. Piattelli, *J. Periodontol.*, 2011, **72**, 1560–1571.
6 T. Shibui, T. Yajima, K. Irie, M. Ochi and Y. Sakakura, *Anat. Sci. Int.*, 2020, 1–8.
7 M. Bohner, G. Baroud, A. Bernstein, N. Döbelin, L. Galea, B. Hesse and J. Sague, *Mater. Today*, 2017, **20**, 106–115.
8 C. Knabe, A. Mele, P. H. Kann, B. Peleska, D. Adel-Khattab, H. Renz and M. Stiller, *Biomater*, 2017, **123**, 48–62.
9 X. Shen, P. Ma, Y. Hu, G. Xu, K. Xu, W. Chen and K. Cai, *J. Mater. Chem. B*, 2016, **4**, 1423–1436.
10 F. Wei, G. Liu, Y. Guo, R. Crawford, Z. Chen and Y. Xiao, *Biomater. Sci.*, 2018, **6**, 2156–2171.
11 V. Likodimos, *Appl. Catal., B*, 2018, **230**, 269–303.
12 H. Zhang, Y. Jiang, Z. Qi, X. Zhong and Y. Yu, *Energy Storage Mater.*, 2018, **12**, 37–43.
13 J. Luo, M. Tamaddon, C. Yan, S. Ma, X. Wang, F. Zhou and C. Liu, *J. Mater. Sci. Technol.*, 2020, **49**, 47–55.
14 Q. Zhu, X. Li, Z. Fan, Y. Xu, H. Niu, C. Li and J. Guan, *Mater. Sci. Eng., C*, 2018, **85**, 79–87.
15 S. Malmir, A. Karbalaei, M. Pourmadadi, J. Hamedi, F. Yazdian and M. Navaee, *Carbohydr. Polym.*, 2020, **234**, 115835–115844.
16 Z. Lin, Y. Zhao, P. K. Chu, L. Wang, H. Pan, Y. Zheng and K. W. Yeung, *Biomater*, 2019, **219**, 119372.
17 J. Wei, H. Ping, J. Xie, Z. Zou, K. Wang, H. Xie and Z. Fu, *Adv. Funct. Mater.*, 2020, **30**, 1904880.
18 M. Rasoulianboroujeni, F. Fahimipour, P. Shah, K. Khoshroo, M. Tahriri, H. Eslami and L. Tayebi, *Mater. Sci. Eng., C*, 2019, **96**, 105–113.
19 V. K. H. Bui, D. Park and Y. C. Lee, *Polymers*, 2017, **9**, 21.
20 A. W. Jatoi, I. S. Kim and Q. Q. Ni, *Carbohydr. Polym.*, 2019, **207**, 640–649.
21 B. Li, Y. Zhang, Y. Yang, W. Qiu, X. Wang, B. Liu and G. Sun, *Carbohydr. Polym.*, 2016, **152**, 825–831.
22 R. Ikono, N. Li, N. H. Pratama, A. Vibriani, D. R. Yuniarni, M. Luthfansyah and H. Kagami, *Biotechnol. Rep.*, 2019, **24**, 00350.
23 B. M. Sedelnikova, E. G. Komarova, Y. P. Sharkeev, A. V. Ugodchikova, T. V. Tolkacheva, J. V. Rau, E. E. Buyko, V. V. Ivanov and V. V. Sheikin, *Bioact. Mater.*, 2019, **4**, 224–235.
24 C. Zhou, A. Xu, D. Wang, G. Lin, T. Liu and F. He, *Biomater. Sci.*, 2018, **6**, 1946–1961.
25 H. Jiang, P. Hao, S. Xu, B. Wang and L. Shu, *J. Biomater. Appl.*, 2017, **32**, 561–569.
26 N. A. Ismail, K. A. M. Amin, F. A. A. Majid and M. H. Razali, *Mater. Sci. Eng., C*, 2019, **103**, 109770.
27 Y. Wang, W. Yang, X. Chen, J. Wang and Y. Zhu, *Appl. Catal., B*, 2018, **220**, 337–347.
28 L. Gu, J. Wang, H. Cheng, Y. Du and X. Han, *Chem. Commun.*, 2012, **48**, 6978–6980.
29 P. Tian, H. Hu, H. Wang, X. Liu and C. Ding, *Mater. Lett.*, 2014, **117**, 98–100.
30 J. Archana, M. Navaneethan and Y. Hayakawa, *J. Power Sources*, 2013, **242**, 803–810.
31 V. R. Akshay, B. Arun, S. Dash, A. K. Patra, G. Mandal, G. R. Mutta and M. Vasundhara, *RSC Adv.*, 2018, **8**, 41994–42008.
32 R. G. Nair, S. Mazumdar, B. Modak, R. Bapat, P. Ayyub and K. Bhattacharyya, *J. Photochem. Photobiol., A*, 2017, **345**, 36–53.
33 V. Jeyalakshmi, R. Mahalakshmy, K. R. Krishnamurthy and B. Viswanathan, *Catal. Today*, 2018, **300**, 152–159.
34 A. F. Nogueira, J. R. Durrant and M. A. De Paoli, *Adv. Mater.*, 2001, **13**, 826–830.
35 C. J. Haggerty, C. T. Vogel and G. R. Fisher, *Oral Maxillofac. Surg. Clin.*, 2015, **27**, 203–226.